Toward Lower Contrast Computer Vision *In Vivo* Flow Cytometry

Stacey Markovic, Siyuan Li, Tianxue Zhang, and Mark Niedre

***Abstract*— There are many applications in biomedical research where detection and enumeration of circulating cells (CCs) is important. Existing techniques involve drawing and enriching blood samples and analyzing them *ex vivo*. More recently, small animal "*in vivo* flow cytometry" (IVFC) techniques have been developed, where fluorescently-labeled cells flowing through small arterioles (ear, retina) are detected and counted. We recently developed a new high-sensitivity IVFC technique termed "Computer Vision(CV)-IVFC". Here, large circulating blood volumes were monitored in the ears of mice with a wide-field video-rate near-infrared (NIR) fluorescent camera. Cells were labeled with a membrane dye and were detected and tracked in noisy image sequences. This technique allowed enumeration of CCs *in vivo* with overall sensitivity better than 10 cells/mL. However, an ongoing area of interest in our lab is optimization of the system for lower-contrast imaging conditions, e.g. when CCs are weakly labeled, or in the case higher background autofluorescence with visible dyes. To this end, we developed a new optical flow phantom model to control autofluorescence intensity and physical structure to better mimic conditions observed in mice. We acquired image sequences from a series of phantoms with varying levels of contrast and analyzed the distribution of pixel intensities, and showed that we could generate similar conditions to those *in vivo*. We characterized the performance of our CV-IVFC algorithm in these phantoms with respect to sensitivity and false-alarm rates. Use of this phantom model in optimization of the instrument and algorithm under lower-contrast conditions is the subject of ongoing work in our lab.**

I. Introduction

Enumeration of circulating cells in the blood stream is applicable to many areas of preclinical biomedical research such a cancer metastasis, stem cell therapies, and immunological responses [1, 2]. Detecting and counting circulating cells in small animals is normally performed by extraction and enriching peripheral blood (PB) and analysis via conventional flow cytometry or hemocytometry. However, it is well understood that handling of cell samples can affect cell viability and count accuracy. Moreover, the small sampling volume and frequency (~100 μL once per day in "survival" mouse studies) means that rare cells may escape detection entirely, and that study of cell circulation kinetics over short time spans is extremely difficult. To address these limitations, optical *in vivo* flow cytometry (IVFC) has been developed, which allows noninvasive, continuous sensing of CCs *in situ*. A number of optical designs have been reported in the literature. For example, in fluorescence microscopic IVFC a single arteriole in the mouse ear [3] or retina [4] is illuminated with a laser, and transient "spikes" are detected as labeled CCs pass through the field of view. However, since small arterioles with small flow PB rates are interrogated (~1 μL), very rare CCs (at concentrations below about 10^3 cells /mL) may escape detection entirely [5].

To improve on this accuracy, we recently developed and reported a new high-sensitivity IVFC method termed "computer vision-IVFC" (CV-IVFC) [6]. The underlying strategy of this technique was to increase the sensitivity of IVFC by sampling larger circulating blood volumes simultaneously. To accomplish this, we performed video-rate fluorescence imaging over a relatively large (5 x 5 mm^2) field of view in the mouse ear, wherein 3-4 artery-vein pairs were imaged. The PB flow rate in this area was on the order of 10-20 μL/min, yielding at least an order of magnitude improvement in detection sensitivity. However, image of the large field of view with rare CCs yielded two major challenges: first, this necessitated high illumination intensities and detector gains, resulting in relatively noisy image sequences with significant autofluorescence background. Second, the large field of view meant that individual CCs were on the order of 1-5 pixels with intensity comparable to background. We developed a novel CV algorithm to detect, track and count moving CCs from image sequences. Briefly, this algorithm used two steps: in the first, candidate CCs were identified, and in the second these were dynamically analyzed in image sequences to yield "cell tracks". When tested *in vivo* with circulating multiple myeloma (MM) cells labeled with a NIR membrane dye, we showed that our CV-IFVC instrument could detect CCs at concentrations lower than 10 cells/mL.

However, an ongoing area of interest in our lab is the use of our CV-IVFC instrument in conditions with lower-contrast. For example, use of cells labeled with GFP would be extremely useful for many applications (due to the ubiquity of GFP labeled cell lines), however, it is known that use of green (versus NIR) laser light will increase tissue autofluorescence and potentially degrade the performance of our system. Likewise, anti-body targeted injected contrast agents are extremely attractive for study of CCs in vivo, but these are likely to yield worse contrast than membrane-bound labels. Therefore, the motivation for this work was to study and optimize CV-IVFC performance with lower contrast between the CCs and background tissue. In this paper, we first briefly review the instrument and algorithms used in CV-IVFC. Second, we describe our ongoing efforts to develop optical phantoms to allow characterization of the instrument in controlled conditions with varying levels of background contrast and structure. We analyzed image

Research supported in part by the National Institutes of Health (R21HL098750; NHLBI) and Massachusetts Life Sciences Center.

S. Markovic is a Graduate Student, Department of Electrical and Computer Engineering, Northeastern University, Boston, MA, 02115, USA, markovic.s@husky.neu.edu.

S. Li and T. Zhang are Undergraduate Students, Department of Electrical and Computer Engineering, Northeastern University, Boston, MA, 02115, USA, li.siyu@husky.neu.edu and zhang.tianx@husky.neu.edu.

M. Niedre is an Assistant Professor, Department of Electrical and Computer Engineering, Northeastern University, Boston, MA, 02115, USA, mniedre@ece.neu.edu.

978-1-4244-7929-0/14/$26.00 ©2014 IEEE

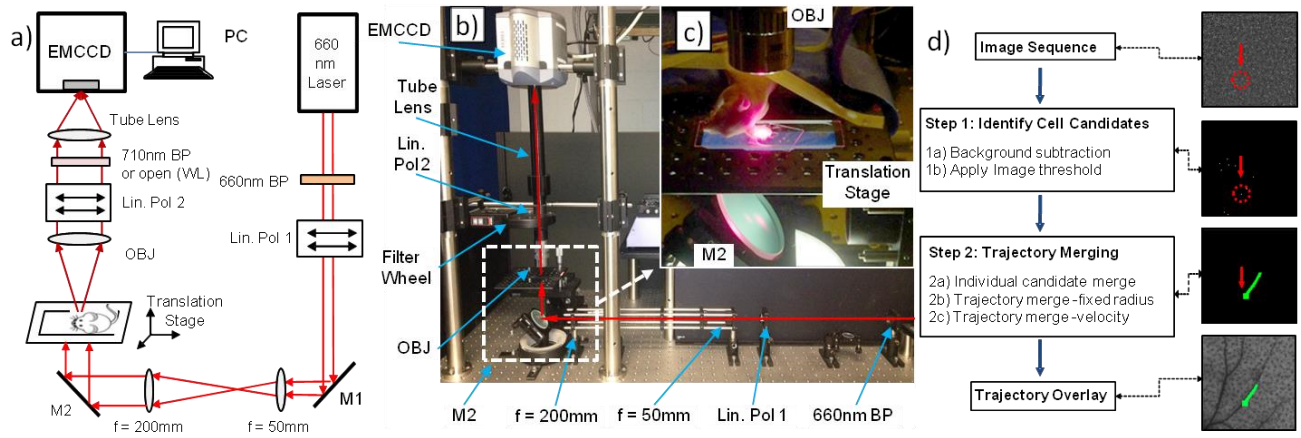

Figure 1. a) Schematic and b) photograph of CV-IVFC system. M, mirror; Lin. Pol, linear polarizer; Obj, 2X objective. c) Photograph of the stage with a mouse ear illuminated for in vivo experiments. d) Computer vision algorithm flow chart.

sequences obtained with these phantoms and showed that we were able to closely replicate conditions observed *in vivo*. We then evaluated the performance of the CV-IVFC algorithm with respect to sensitivity and false alarm rate (FAR). Use of these phantoms in the optimization of our system is the subject of ongoing work in our lab.

II. Methods and Materials

A. CV-IVFC Overview

A schematic and photograph of the system are shown in Figs. 1a,b respectively. A sample (phantom or mouse ear) was placed on a translation stage as shown in fig. 1c and then trans-illuminated with a 660 nm diode laser to excite a near infrared dye chosen to take advantage of the relatively low tissue autofluorescence and light attenuation. A 660 nm "clean-up" filter eliminated any stray out of band light from the diode-pumped solid state laser, and then the beam was expanded using a plano-convex lens pair. The beam at the sample was approximately Gaussian with 5 mm waist with average intensity of 10 mW/cm^2. Light was collected from the sample with a 2X objective and 1X tube lens. Fluorescence image sequences were collected with a 710 nm filter in place (white light images were collected by removing this filter). Images were recorded with a 14-bit electron multiplied charge coupled device (EMCCD) camera. The gain on the EMCCD was used to amplify the relatively low fluorescence emission intensity of cells in the large field of view but also resulted in relatively high imaging noise and background intensity.

We developed a novel CV algorithm to automatically detect and track cells from the resulting noisy fluorescence image sequences. The flow chart for this algorithm is shown in figure 1d. Briefly, this algorithm used two major analysis steps. In step one, pixels or groups of pixels exceeding a set threshold were identified as "cell candidates". 14-bit fluorescence images (figs. 2a-c) were converted to a binary image sequence by choosing a threshold T. Pixels or pixel groups exceeding this threshold were set to '1', and pixels below this threshold were set to zero (figs. 2d-f). The choice of threshold was critical and was chosen to be a percentile of all pixel intensities in an image sequence; we determined heuristically that threshold values in the range of 99.93 to 99.99 of the maximum worked well *in vivo*.

In step two, the dynamic behavior of cell candidates between successive image frames was analyzed so that cells could be merged into tracks. A full description is found in [6], but in brief, when cell candidates were identified, spatial regions related to the previously known speed and direction of the cell were searched in subsequent image frames. These were merged into tracks. Since cells would periodically disappear in image frames (due to variations in intensity), images were searched for up to 15 frames (i.e. 0.8s) following the last known location of the cell candidates. Cell candidates which appeared in individual frames only were discarded, and cell candidates which formed tracks were recorded by the algorithm (fig 2g-i). In this way, the CV-IVFC instrument and algorithm could detect number, trajectory and speed of CCs which appeared in the field of view. The code took 2.5 minutes to execute per 1,000 frames in MATLAB on a 64-bit personal computer with 16 GB of RAM.

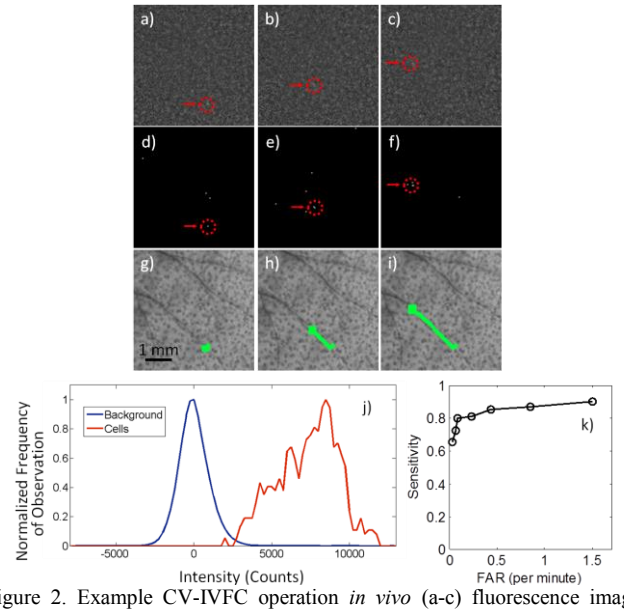

Figure 2. Example CV-IVFC operation *in vivo* (a-c) fluorescence image acquired at 3 times separated by 0.5s (d-f) binary thresholded images (after algorithm Step 1) (g-i) dynamic cell tracks determined in step 2, overlaid on white light images of ear vasculature. (j) Histogram of background and cell pixel intensities in an image sequence after background subtraction. (k) Performance of the CV-IVFC algorithm with respect to sensitivity and FAR for varying thresholds in Step-1.

The performance of the algorithm could be adjusted using a number of parameters related to dynamic analysis (Step-2) and threshold level (Step-1). An example histogram of the pixel values for background intensity (after mean subtraction) and cell intensity values for an image sequence are shown in figure 2j. Selection of the threshold value in Step-1 impacted the overall performance with respect to sensitivity and false alarm rate (FAR) as described in section D below. For example, selection of a higher threshold resulted in a lower FAR, but reduced sensitivity (fig 2k).

B. Performance of CV-IVFC with Varying Contrast

We are interested in characterizing and optimizing of the CV-IVFC instrument and algorithm in imaging conditions with varying contrast. For example, in conditions with less-bright fluorophore labeling the red histogram in fig 2j (cells) is expected to shift to the left, whereas higher background autofluorescence is expected to increase the width of the blue histogram (background). The impact of this on the instrument performance (fig 2k) is not well understood, but we expect to degrade performance. In the current work, we developed a phantom model to closely mimic in vivo imaging conditions, so that we could test and characterize the instrument performance under controlled conditions. Optimizing the algorithm to improve performance under these conditions is the subject of ongoing work.

C. Phantom Preparation

Tissue-mimicking phantoms were made with polyester resin, TiO_2, and India Ink to simulate approximate optical properties of tissue at 700 nm with reduced scattering coefficient $\mu'_s = 15$ cm^{-1} and absorption coefficient $\mu_a = 0.1$ cm^{-1} [7]. These were placed in a mold to mimic the approximate size of a mouse ear (20 mm diameter, 2 mm thick), with a strand of Tygon tubing inserted to simulate a large blood vessel (fig 3). Inspection of *in vivo* image sequences (fig 2a-c) showed that sebaceous glands in the ear of the mouse appear as discrete point autofluorescent objects, specifically, an average of 65 sebaceous glands were present over a set of 12 mice that were tested previously. To replicate this in phantoms, 6 μm diameter fluorescent microspheres were added to the resin before hardening; either 0, 850 or 1,700 spheres/mL were added to a volume of 10 mL of phantom material. In order to mimic the background autofluorescence, 0.4 μM of Alexafluor-680 dye was added to the resin. To simulate blood flow, a solution of PBS and the microspheres, representing fluorescent "cells" matching the spectra of Cyanine 5.5 and Alexafluor-680 dyes, were pumped through the tube via a syringe pump at a flow speed of 1.7 mm/s. Tests were run with microspheres at concentrations of 2 x 10^3 spheres/mL, EMCCD gain of 10-30 (of a maximum of 300), exposure time 0.05s, frame rate of 19 frames/s, and a total of 1,000 frames per sequence. Measurements were repeated continuously so that data was collected for 20 minutes for each phantom.

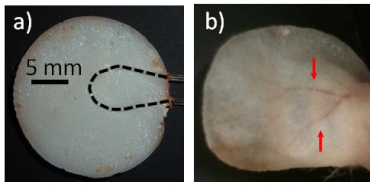

Figure 3. a) Photograph of an example ear-mimicking phantom with a dotted line showing the Tygon tubing position. B) Photograph of an example the mouse ear for comparison.

D. Performance Metrics

Background and sphere intensities from image sequences for each phantom were analyzed. Histograms of pixel intensities were plotted after pixel-by-pixel background mean subtraction. Microspheres were tracked with our CV-IVFC algorithm as we have described previously, and sensitivity and FAR performance was quantified for each phantom. Here, sensitivity was calculated as TP/(TP + FN), here TP were the true positives count (determined by a human operator) and FN were the false negative counts, i.e. cells missed by the algorithm. The human operator manually counted the number and arrival time of spheres which took approximately 45 minutes per 20 minutes of phantom data. The operator performed manual counting before running the CV-IVFC code to minimize potential bias. Finally, the operator verified that the counts reported by the algorithm corresponded to spheres which took 30 minutes per data set. The FAR was calculated as the number of false positives (FP) incorrectly detected by the algorithm per minute. The performance was recomputed for a range of threshold percentages in Step-1 of the CV algorithm, specifically, 99.93 to 99.99 of maximum.

III. RESULTS

An example set of fluorescence images for a phantom with high contrast (no embedded spheres or AF-680 dye added) and low contrast (1,700 spheres/mL and 0.4 μM AF-680 added) are shown in figs. 4a-c and 4j-l, respectively. By inspection, addition of the contrast materials resulted in an image sequence that qualitatively better matched that observed *in vivo*. The effect of this contrast on Step-1 (cell candidate identification) is clearly observed in figs 4d-f and 4m-o, respectively; a significantly higher number of false-candidates are indicated. However, the CV algorithm was successful in identifying the moving microspheres for both cases as shown in figs 4g-i and 4p-r.

To better quantify this effect, we computed the pixel-intensity histograms and algorithm tracking performance (sensitivity vs. FAR) for all of the phantoms we tested. Example data is shown in figure 5. Intensity histograms for a high-contrast, medium contrast and low-contrast phantom are shown in figs 5a-c, respectively. For the high-contrast phantom, the background mean and standard deviation were 0 and 103 counts while the spheres had a mean of 12,583 counts and standard deviation of 4,496 counts (fig 5a). For the low-contrast phantom the background intensity had a mean of 0 and standard deviation of 763 counts and sphere intensities with a mean of 5,500 and standard deviation of 1,462 counts (5c). Comparison of the fig 2j verifies that the low-contrast phantom closely approximated what was observed in mice *in vivo*.

Last, the performance of the CV-IVFC algorithm with respect to sensitivity and FAR for two example phantoms are shown in fig 4d, along with corresponding *in vivo* data. As such the overall system performance observed in the low-contrast phantom more similarly replicated the in vivo

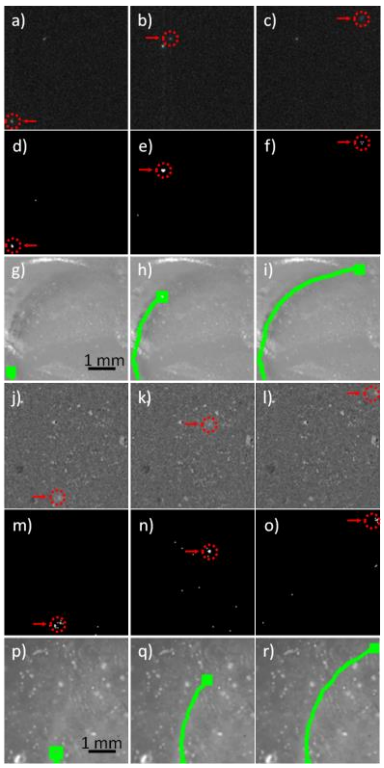

Figure 4. Example fluorescence image sequences for a high-contrast (a-c) and low-contrast (j-l) phantom, respectively, with frames separated by 0.25 s. (d-f, m-o) corresponding thresholded image sequences are shown, indicted microsphere candidates identified in Step-1 of the algorithm. (g-i, p-r) extracted tracks and white-light overlay images for the high- and low-contrast phantoms, respectively.

performance of the algorithm. For example, for one operating threshold (99.96th percentile), the low contrast phantom had sensitivity of 0.95 and FAR of 0.84 spheres/min whereas the *in vivo* performance had a sensitivity of 0.81 and FAR of 0.24 cells/min.

IV. Discussion and Conclusion

We previously reported development and validation of a novel high-sensitivity computer vision system and algorithm for detecting, tracking and counting rare CCs at concentrations below 10 cells / mL in vivo. In this work, we were successful in developing a phantom model that closely replicated both the qualitative (appearance) and quantitative (intensity histogram) properties of previously measured *in vivo* data. The sensitivity was higher for phantoms than *in vivo* due to the spheres being twice as bright as labeled MM cells [8]. The FAR was higher in the phantom results compared to *in vivo* data due to a higher number of stationary noisy pixels being merged as cell tracks. As noted, the fluorescent labeling (contrast) of MM cells in our previous *in vivo* studies was relatively "bright" compared to that expected, e.g. with constitutively expressed fluorescent proteins or receptor targeted fluorescent dyes. Ongoing work in the lab incorporates these low contrast phantoms with spheres of lower intensities to mimic different cell labeling techniques. We expect that the phantom models developed here will allow us to test and refine optimization strategies for lower-contrast imaging conditions, for example, by modifying the dynamic tracking analysis in Step-2 of the CV

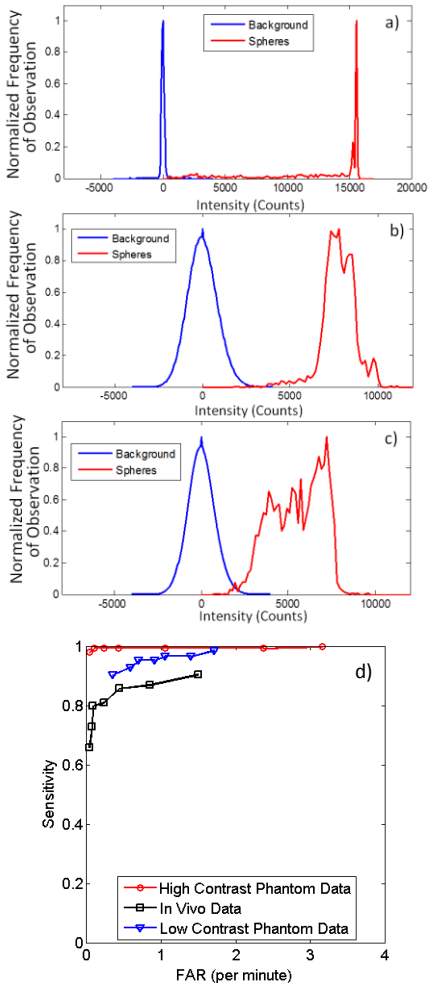

Figure 5. Pixel-intensity histograms for example a) high, b) medium, and c) low-contrast phantoms. (d) Sensitivity versus FAR performance for an example high- and low-contrast phantom, as well as *in vivo* data.

algorithm. These phantoms provide a platform to test new cell labeling techniques ex-vivo with confidence before proceeding to costly and time consuming animal studies. Robust operation with arbitrary cell-labeling strategies is expected to increase the overall utility CV-IVFC in the study of rare CCs for many pre-clinical research applications.

References

[1] M. Cristofanilli, et al., "Circulating tumor cells, disease progression, and survival in metastatic breast cancer," *N Engl J Med*, vol. 351, no. 8, pp. 781-91, 2004.

[2] C. Lo Celso, et al., "Live-animal tracking of individual haematopoietic stem/progenitor cells in their niche," *Nature*, vol. 457, pp. 92–6, 2009.

[3] J. Novak, et al., "In vivo flow cytometer for real-time detection and quantification of circulating cells," *Opt Lett*, vol. 29(1), pp. 77-9,2004.

[4] C. Alt, et al., "Retinal flow cytometer," *Opt Lett*, vol. 32(23), pp. 3450-2, 2007.

[5] V.V. Tuchin, A. Tarnok, and V.P. Zharov, "In Vivo Flow Cytometry: A Horizon of Opportunities," *Cytometry A*, vol. 79A, no. 10, pp. 737–745, 2011.

[6] S. Markovic, et al., "A Computer Vision Approach to Rare Cell In Vivo Fluorescence Flow Cytometry," *Cytometry A*, vol. 83A, pp. 1113-1123, 2013.

[7] J. Baeten, et al., "Development of fluorescent materials for Diffuse Fluorescence Tomography standards and phantoms," *Opt Express*, vol. 15, no. 14, pp. 8681-94, 2007.

[8] E. Zettergren, et al., "Instrument for fluorescence sensing of circulating cells with diffuse light in mice *in vivo*, " *J Biomed Opt,* vol. 17, no. 3, pp. 037001, 2012.